Nonlinear Compton scattering of ultrashort intense laser pulses

D. Seipt* and B. Kämpfer†
Helmholtz-Zentrum Dresden-Rossendorf, P.O. Box 510119, D-01314 Dresden, Germany
(Received 15 October 2010; published 4 February 2011)

The scattering of temporally shaped intense laser pulses off electrons is discussed by means of manifestly covariant quantum electrodynamics. We employ a framework based on Volkov states with a time-dependent laser envelope in light-cone coordinates within the Furry picture. An expression for the cross section is constructed unambiguously in respect of the pulse length. A broad distribution of scattered photons with a rich pattern of subpeaks like that obtained in Thomson scattering is found. These broad peaks may overlap at sufficiently high laser intensity, rendering inappropriate the notion of individual harmonics. The limit of monochromatic plane waves as well as the classical limit of Thomson scattering are discussed. As a main result, a scaling law is presented connecting the Thomson limit with the general result for arbitrary kinematics. In the overlapping regions of the spectral density, the classical and quantum calculations give different results, even in the Thomson limit. Thus, a phase-space region is identified where the differential photon distribution is strongly modified by quantum effects.

DOI: 10.1103/PhysRevA.83.022101 PACS number(s): 12.20.Ds, 41.60.−m

I. INTRODUCTION

The use of chirped-pulse amplification [1] has led to a prodigious advance in available laser power. The current records reach several petawatts, and accompanying interest in strong-field physics culminates in planned large-scale laser facilities such as the anticipated "Extreme Light Infrastructure" (ELI) [2]. The pioneering theoretical studies in strong-field physics considered both pair creation in a strong field [3] and the cross-channel process, electron-photon scattering [4–10], dubbed nonlinear Compton scattering, where the use of laser beams has already been suggested. Since then there has been a wealth of theoretical papers and we refer the reader to the reviews [11–16]. In nonlinear Compton scattering

$$e(p) + \ell\gamma_L(k) \to e'(p') + \gamma(k'), \tag{1}$$

a number ℓ of photons, each with four-momentum $k = \omega(1, \mathbf{n})$, from a high-intensity laser, where ω is the laser frequency and $\mathbf{n}$ is the laser propagation axis, scatter off an electron (mass m) with four-momentum $p = (E_p, \mathbf{p}) = m\gamma(1, \boldsymbol{\beta})$ (where $\gamma = E_p/m = 1/\sqrt{1-\boldsymbol{\beta}^2}$ is the relativistic Lorentz factor and $\boldsymbol{\beta} = \mathbf{p}/E_p$ denotes the reduced velocity), producing a single photon with four-momentum $k' = \omega'(1, \mathbf{n}')$, emitted with frequency ω' in the direction $\mathbf{n}' = (\cos\varphi\sin\theta, \sin\varphi\sin\theta, \cos\theta)$. The final-state electron has the four-momentum $p' = (E_{p'}, \mathbf{p}')$.

A convenient measure of laser intensity is the dimensionless laser amplitude $a \equiv eE/m\omega$, with E being the root-mean-square electric field. $|e|$ denotes the elementary charge. The parameter a is a purely classical quantity, representing the work performed by the field on the electron in one wavelength. Thus, a is the classical nonlinearity parameter [17] and it is related to the ponderomotive potential $U_p = ma^2/2$. The definition of a can be made explicitly Lorentz and gauge invariant [18]. When a becomes of order unity the quiver motion of the electron in the laser beam becomes relativistic in a classical picture.

The spectrum of nonlinear Compton scattering has been observed in several experiments colliding laser and electron beams, such as low-intensity laser photons ($a = 0.01$) with low-energy ($\sim$1 keV) electrons from an electron gun [19], $a = 2$ photons with plasma electrons from a gas jet [20], and, more recently, subterawatt photons ($a = 0.35$) from a CO_2 laser with 60 MeV electrons from a linac at the BNL Accelerator Test Facility [21]. Using linearly polarized photons the latter two experiments [20,21] have analyzed the characteristic azimuthal intensity distributions, confirming quadrupole and sextupole patterns for the second and third harmonics, respectively. Recently, the energy spectrum of the scattered radiation has been measured in an all-optical setup using laser-accelerated electrons [22].

Probably the best-known experiment is SLAC E-144, probing strong-field QED using a terawatt Nd:glass laser ($a \simeq 0.6$) in conjunction with high-energy (46.6 GeV) electrons [23]. The observation of nonlinear Compton scattering has been reported [24] as well as the observation of the crossed process of nonlinear pair creation, due to the interaction of a Compton scattered high-energy photon with a second laser beam [25].

The low-energy limit (in terms of laser frequency) of Compton scattering is Thomson scattering, which is described completely classically [26,27]. This classical picture is used as the theoretical framework for many applications of laser Compton scattering such as x-ray sources [28–30] or diagnostic tools [31]. A convenient parameter to distinguish the two regimes is the quantity

$$y_\ell = \frac{s_\ell - m^2}{m^2} = \frac{2\ell k\cdot p}{m^2}, \tag{2}$$

where $s_\ell = (p + \ell k)^2$ expresses the center-of-mass energy squared for the generation of the ℓth harmonic in a Lorentz-invariant manner.[1] The $\ell + 1 \to 2$ process is kinematically

*d.seipt@hzdr.de
†kaempfer@hzdr.de

[1] p and k are four-vectors; thus $k\cdot p$ denotes a scalar product; we employ units with $\hbar = c = 1$.

equivalent to the scattering of one photon with momentum ℓk off an electron with momentum p; thus it appears as a (pseudo) $2 \to 2$ process. The Thomson regime is recovered for $y_\ell \ll 1$, while for $y_\ell > 1$ one finds striking differences from the Thomson scattering. The electron recoil during the scattering may be quantified by the Lorentz-invariant quantity $t = (p - p')^2$ which is in the range $0 \leqslant -t \leqslant m^2 \frac{y_\ell^2}{1+y_\ell}$, i.e., in the Thomson regime $-t/m^2 \ll 1$ holds.

A quantity measuring nonlinear quantum effects,

$$\chi_R = \frac{e\sqrt{(F^{\mu\nu}p_\nu)^2}}{m^3} = \frac{1}{2}ay_1, \tag{3}$$

has been introduced in [4,8]. It measures the work done by the field over the Compton wavelength m^{-1} in the rest frame of the initial electron. Introducing the critical field strength [32] $E_S = m^2/e = 1.3 \times 10^{18}$ V/m, this may also be written as $\chi_R = E_\star/E_S$, where $E_\star$ is the rms electric field strength in the electron's rest frame. The parameter χ_R combines nonlinearity and quantum effects. χ_R is of the order of unity if both a and y_1 are of the order of unity. Thus, the corrections to the classical description (Thomson scattering) are important if either (i) an intense high-energy photon pulse, e.g., produced by an x-ray free-electron laser, interacts with low-energy electrons, or (ii) a multi-GeV electron beam is brought into collision with an optical high-intensity laser. The latter scenario is similar to the SLAC E-144 experiment but with a higher value of a. For the 50 GeV SLAC beam in conjunction with a counterpropagating optical laser ($\omega \sim 1$ eV) one has $y_\ell \sim 1$. These parameters will be used mainly below for numerical calculations. The FACET project [33] at SLAC envisages investigations within such kinematics in line with (ii).

Intense lasers use short pulses (few femtosecond, few laser cycles) requiring a proper treatment of the laser pulse structure. Rich substructures of the scattered photon spectra were predicted within the classical picture [34–37] of Thomson scattering. These substructures have not yet been confirmed experimentally. The effect of radiation back reaction on the spectra was studied in [38] and found to be important. Only a few publications address quantum calculations in pulsed fields for scalar particles [39] and for spinor particles [40,41]. In [42], a connection between the emitted angular spectrum in nonlinear Compton scattering and the carrier envelope phase in few-cycle laser pulses was established. In a related field, electron wave-packet dynamics in strong laser fields has been studied in, e.g., [43,44].

In our paper we calculate the emitted photon spectrum in nonlinear Compton scattering using a generalized Volkov solution with temporal shape in light-cone coordinates. The aim of our study is to compare the QED calculations for nonlinear Compton scattering with results from a classical calculation, i.e., Thomson scattering. Our paper is organized as follows. In Sec. II we present Volkov states in pulsed laser fields. Section III continues with the calculation of the matrix element and the transition probability. A slowly-varying-envelope approximation is discussed. Numerical results are presented in Sec. IV. We discuss various limiting cases of our general results, including monochromatic plane waves and the Thomson limit. As a main result, a scaling law is presented, connecting the Thomson spectrum with the Compton spectrum. In the Appendix we present the Fourier transformation of the Volkov state which furnishes a representation of the S matrix in momentum space.

II. TEMPORALLY SHAPED VOLKOV STATES

A strong laser field may be considered as a coherent state of photons $|\mathcal{C}\rangle$, characterized by the polarization and momentum distribution $\mathcal{C}^\mu(k)$, if the depletion of the laser photons from $|\mathcal{C}\rangle$ by an interaction process with electrons is negligible, i.e., for any relevant scattering process $S = \langle \text{out}; \mathcal{C}'|S|\text{in}; \mathcal{C}\rangle$ with $\mathcal{C}' = \mathcal{C}$ is valid, where "in" and "out" are particle number states without coherent parts [45]. Then, it is possible to work within the Furry picture [46], where the interaction of an electron with the classical background field $A^\mu(x)$, which is the Fourier transform of $\mathcal{C}^\mu(k)$, is treated nonperturbatively and solutions of the Dirac equation

$$(i\partial\!\!\!/ - eA\!\!\!/ - m)\psi(x) = 0 \tag{4}$$

are utilized as basic "in" and "out" states for the perturbative expansion of the S matrix. For background fields in the form of plane waves, closed solutions of (4) can be found,

$$\psi_{p,s}(x) = \left(1 + \frac{e}{2k\cdot p}\, k\!\!\!/\, A\!\!\!/\right) \exp\{iS_p(x)\}\frac{u_{p,s}}{\sqrt{2E_p}}, \tag{5}$$

where the free Dirac spinor for momentum p and spin s fulfills $(p\!\!\!/ - m)u_{p,s} = 0$ and is normalized to $\bar{u}_{p,s'}u_{p,s} = 2m\delta_{ss'}$. The phase is the classical Hamilton Jacobi action

$$S_p(x) = -p\cdot x + f(k\cdot x), \tag{6}$$

with $f = f_1 + f_2$, $f_1 = -\int_{\phi_0}^{k\cdot x} d\phi \frac{eA\cdot p}{k\cdot p}$ and $f_2 = \int_{\phi_0}^{k\cdot x} d\phi \frac{e^2A^2}{2k\cdot p}$. Equation (5) represents the famous Volkov states, whose perturbative expansion in terms of interactions with the laser field is depicted in Fig. 1 of [45] (the expansion parameter, i.e., the coupling strength at the vertices, is a_0 defined below).

For the vector potential we use a real transverse plane wave

$$A^\mu = A_0\, g(k\cdot x)\,(\epsilon_1^\mu \cos\xi \cos k\cdot x + \epsilon_2^\mu \sin\xi \sin k\cdot x), \tag{7}$$

modified by an envelope function g and fulfilling $A\cdot k = 0$ and $k\cdot k = 0$. The parameter ξ determines the polarization of the laser: It is linearly x (y) polarized for $\xi = 0$ ($\xi = \pi/2$) and circularly polarized for $\xi = \pm\pi/4$. For other values of ξ, the laser is elliptically polarized [47]. The vector potential is normalized such that the mean energy density or the energy flux $\langle \mathbf{E}^2\rangle \propto -A_\mu A^\mu = g^2A_0^2/2$, where $\langle\cdots\rangle$ means averaging over the fast oscillations of the carrier wave, is independent of ξ, but the dimensionless laser amplitude a, as defined in the Introduction, is time dependent. A time-independent laser strength parameter may be defined by the normalized peak value of the vector potential $a_0 = eA_0/m$ (with this definition, $a^2 = a_0^2/2$ for $g \equiv 1$). The vector potential (7′) can also be cast into a complex form,

$$A^\mu = \frac{A_0 g(k\cdot x)}{2}\left(\epsilon_+^\mu e^{-ik\cdot x} + \epsilon_-^\mu e^{+ik\cdot x}\right) = \frac{A_0 g}{2}B^\mu, \tag{7′}$$

with the complex polarization vectors $\epsilon_\pm^\mu = \cos\xi\epsilon_1^\mu \pm i\sin\xi\epsilon_2^\mu$ and $\epsilon_+\cdot\epsilon_- = -1$, $\epsilon_\pm\cdot\epsilon_\pm = \sin^2\xi - \cos^2\xi$, and the definition $B^\mu = \epsilon_+^\mu e^{-ik\cdot x} + \epsilon_-^\mu e^{+ik\cdot x}$.

In what follows, the temporal pulse shape will often be chosen as a hyperbolic secant pulse,

$$g(k\cdot x)=\frac{1}{\cosh\left(\frac{k\cdot x}{\sigma}\right)}, \tag{8}$$

with width σ, or a Gaussian

$$g(k\cdot x)=\exp\left\{-\frac{(k\cdot x)^2}{2\sigma^2}\right\}. \tag{9}$$

In addition to these special cases, any other smooth function g which depends solely on $k\cdot x$ is possible.

Since the vector potential A^μ depends only on $k\cdot x$, it is convenient to work in light-cone coordinates [39,41], defined with respect to the lightlike four-vector $n_+=k/\omega=(1,\mathbf{n})$. We will always choose the coordinate system such that the laser pulse propagates along $\mathbf{n}=(0,0,-1)$. Then the light-cone components of a four-vector B^μ may be defined by a projection via

$$B_+\equiv B\cdot n_+=B_0+B_3,\quad B_-\equiv B\cdot n_-=B_0-B_3, \tag{10}$$

$$\mathbf{B}_\perp\equiv(B_1,B_2) \tag{11}$$

with $n_-^\mu=(1,-\mathbf{n})$. In these new coordinates, the scalar product reads $A\cdot B=\frac{1}{2}(A_+B_-+A_-B_+)-\mathbf{A}_\perp\cdot\mathbf{B}_\perp$. Arranging these components as a four-vector $B=(B_+,B_-,\mathbf{B}_\perp)$, one may introduce a nondiagonal metric

$$g_{\mu\nu}=\begin{pmatrix}0&\frac{1}{2}&0&0\\ \frac{1}{2}&0&0&0\\ 0&0&-1&0\\ 0&0&0&-1\end{pmatrix} \tag{12}$$

with determinant $\sqrt{-g}=1/2$; thus the Lorentz-invariant volume element is $\sqrt{-g}d^4x=\frac{1}{2}dx_+dx_-d^2\mathbf{x}_\perp$. The inverse transformation is given by $B_0=\frac{1}{2}(B_++B_-)$, $B_3=\frac{1}{2}(B_+-B_-)$. With this convention for light-cone coordinates, the relation $k\cdot x=\omega x_+$ holds, and the conjugate momentum to x_+ is P_-, and vice versa. The mass-shell relation or free-particle dispersion relation $E_p^2=\mathbf{p}^2+m^2$ reads

$$p_-=\frac{\mathbf{p}_\perp^2+m^2}{p_+}. \tag{13}$$

In these coordinates, the Volkov wave function (5) reads

$$\psi_{p,s}(x)=C_p(\mathbf{x}_\perp,x_-,x_+)\frac{u_{p,s}}{\sqrt{2E_p}}, \tag{14}$$

$$C_p(\mathbf{x}_\perp,x_-,x_+)=[1+d_pg(x_+)(\not k\not\epsilon_-e^{i\omega x_+}+\not k\not\epsilon_+e^{-i\omega x_+})]\times e^{-\frac{i}{2}(p_+x_-+p_-x_+)+i\mathbf{p}_\perp\cdot\mathbf{x}_\perp+if(x_+)} \tag{15}$$

with $d_p=a_0m/(4k\cdot p)$. Some details of the Volkov solution (14) and (15) are considered in [49] (cf. Figs. 1 and 2 therein). For instance, the effect of the laser pulse is a local deformation of the electron wave fronts due to the buildup of an effective, time-dependent momentum $q^\mu(x_+)=p^\mu+g^2(x_+)b_pk^\mu$ with $b_p=m^2a_0^2/4k\cdot p$. The momentum $q^\mu(x_+)$ achieves its maximum at the center of the laser pulse, $x_+=0$. Thus, inside the laser pulse, especially for $x_+=0$, the fully dressed electron wave function behaves as $\propto e^{-iq\cdot x}=e^{-i(m+b_p\omega_\star)t+ib_p\omega_\star z}$ in a reference frame comoving with the initial electron outside the laser pulse, i.e., $p=(m,0,0,0)$, in contrast to the free-electron wave function $\propto e^{-ip\cdot x}=e^{-imt}$, i.e., the electron wavelength changes and the wave fronts become tilted. Both effects are proportional to the ponderomotive potential, i.e., $\propto b_p\omega_\star=ma_0^2/4=U_p/2$, where $\omega_\star=p\cdot k/m$ is the laser frequency in the frame comoving with the initial electron.

III. CALCULATION OF THE MATRIX ELEMENT

A. The *S* matrix

The interaction of the Volkov electron e_V with photon modes different from the laser field is treated by a perturbative S matrix expansion. The Born approximation of the matrix element for the emission of one photon, i.e., nonlinear Compton scattering $e_V(p)\to e_V(p')+\gamma(k')$, is depicted in Fig. 1. Using Feynman rules [48], the S matrix element for such a process is given by

$$S_{fi}=\langle p',s';k',\epsilon'_{\lambda'}|S[A]|p,s\rangle=-ie\int d^4x\bar\psi_{p',s'}(x)\frac{e^{ik'\cdot x}}{\sqrt{2\omega'}}\not\epsilon'_{\lambda'}\psi_{p,s}(x), \tag{16}$$

which reads in light-cone coordinates, suppressing spin (s,s') and polarization indices of the outgoing photon (λ') from now on,

$$S_{fi}=N_0\int d^4x\bar u_{p'}(1+d_{p'}g\not B\not k)\times\not\epsilon'(1+d_pg\not k\not B)u_pe^{i(S_p-S_{p'}+k'\cdot x)} \tag{17}$$

$$=\frac{N_0}{2}\int d^2\mathbf{x}_\perp dx_+dx_-\,\Gamma(x_+)\,e^{iH(x_+,x_-,\mathbf{x}_\perp)} \tag{18}$$

with $N_0=-ie/\sqrt{2\omega'2E_p2E_{p'}}$ and

$$\Gamma(x_+)=\mathscr{T}_0^0+g\,e^{i\omega x_+}\mathscr{T}_1^1+g\,e^{-i\omega x_+}\mathscr{T}_{-1}^1+g^2\,\mathscr{T}_0^2+g^2\,e^{2i\omega x_+}\mathscr{T}_2^2+g^2\,e^{-2i\omega x_+}\mathscr{T}_{-2}^2, \tag{19}$$

where

$$\mathscr{T}_0^0=\bar u_{p'}\not\epsilon'u_p, \tag{20}$$

$$\mathscr{T}_{\pm1}^1=\bar u_{p'}(d_{p'}\not\epsilon_\mp\not k\not\epsilon'+d_p\not\epsilon'\not k\not\epsilon_\mp)u_p, \tag{21}$$

$$\mathscr{T}_0^2=4(k\cdot\epsilon')d_pd_{p'}\bar u_{p'}\not ku_p, \tag{22}$$

$$\mathscr{T}_{\pm2}^2=d_pd_{p'}\bar u_{p'}(\not\epsilon_\mp\not k\not\epsilon'\not k\not\epsilon_\mp)u_p. \tag{23}$$

Because $\not\epsilon_\mp\not k\not\epsilon'\not k\not\epsilon_\mp=-2(\epsilon'\cdot k)(\epsilon_\mp\cdot\epsilon_\mp)\not k$, one finds $\mathscr{T}_{\pm2}^2=0$ for circular polarization. Furthermore,

$$H(x_+,x_-,\mathbf{x}_\perp)=S_p-S_{p'}+k'\cdot x=(p'+k'-p)\cdot x+f(x_+)-f'(x_+) \tag{24}$$

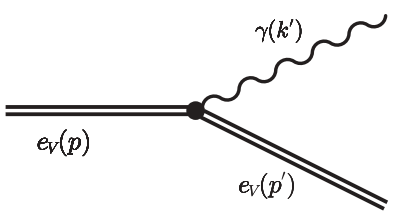

FIG. 1. Feynman diagram for nonlinear Compton scattering as the decay of a laser dressed Volkov electron state.

with $f' = f(p \to p') = f_1(p') + f_2(p')$ and

$$f_1(x_+;p) = -\frac{ma_0}{k\cdot p}\int_{\phi_0}^{k\cdot x} d\phi\, g(\phi)[p\cdot\epsilon_1 \cos\xi\cos\phi + p\cdot\epsilon_2 \sin\xi\sin\phi], \tag{25}$$

$$f_2(x_+;p) = -\frac{m^2a_0^2}{2k\cdot p}\int_{\phi_0}^{k\cdot x} d\phi\, g^2(\phi)[\cos^2\xi\cos^2\phi + \sin^2\xi\sin^2\phi]. \tag{26}$$

Inspecting Eq. (24), it is obvious that the dependence of H on x_- and $\mathbf{x}_\perp$ is trivial and the integrations over these variables in Eq. (18) can be done analytically. As a result, momentum conservation is imposed on the components $p'_+ = p_+ - k'_+$ and $\mathbf{p}'_\perp = \mathbf{p}_\perp - \mathbf{k}'_\perp$, and the exponent

$$H_+(x_+) = \tfrac{1}{2}(k'_- + p'_- - p_-)x_+ + f(x_+) - f'(x_+) \tag{27}$$

remains. Due to the nontrivial pulse-dependent structure of H_+, the x_+ integration does not yield another conservation law. Thus, the frequency of scattered photons ω' is not fixed by energy and momentum conservation as a function of scattering angle θ, i.e., ω' remains as independent parameter. Including the x_+ dependence of $\Gamma(x_+)$, some rather complicated functions of ω' emerge:

$$\mathscr{A}_N^M = \int_{-\infty}^{\infty} dx_+ g^M(x_+)\exp i\{H_+(x_+) + N\omega x_+\}. \tag{28}$$

With these definitions, the S matrix element can be written as

$$S_{fi} = (2\pi)^3\delta^2(\mathbf{k}'_\perp + \mathbf{p}'_\perp - \mathbf{p}_\perp)\delta(k'_+ + p'_+ - p_+)N_0\mathscr{M} \tag{29}$$

with

$$\mathscr{M} = \mathscr{T}_0^0\mathscr{A}_0^0 + \mathscr{T}_1^1\mathscr{A}_1^1 + \mathscr{T}_{-1}^1\mathscr{A}_{-1}^1 + \mathscr{T}_0^2\mathscr{A}_0^2 + \mathscr{T}_2^2\mathscr{A}_2^2 + \mathscr{T}_{-2}^2\mathscr{A}_{-2}^2. \tag{30}$$

For a derivation in momentum space see the Appendix. The integrals $\mathscr{A}_N^M$ are numerically convergent for $M \geqslant 1$ due to the presence of the pulse function in the integrand, rendering the range of integration practically finite. The integral $\mathscr{A}_0^0$, however, contains a divergent part and must be regularized. A possible method has been proposed in [41], where one multiplies the integrand with a convergence factor $e^{-\varepsilon|x_+|}$, $\varepsilon > 0$, and performs an integration by parts. The result is

$$\mathscr{A}_0^0 = -\frac{2}{P_-}\int_{-\infty}^{\infty} dx_+ \frac{d(f-f')}{dx_+}\exp\{i\,H_+(x_+)\} + 4e^{i[f(0)-f'(0)]}\lim_{\varepsilon\to 0^+}\frac{\varepsilon}{P_-^2+\varepsilon^2} \tag{31}$$

with $P_- = k'_- + p'_- - p_-$. In (31), the first part is now convergent and the second part is proportional to a δ distribution with support at $\omega' = 0$. The latter contribution can be neglected in our analysis for $\omega' > 0$. Physically, this last term relates to the scattering of free electrons in the "in" and "out" states,[2] i.e., the dressed-electron lines are replaced by free-electron lines in the Feynman diagram in Fig. 1, which is forbidden by energy momentum conservation. Consequently, from $\omega' = 0$ follows $k' = 0$; there is no scattering described at all by this contribution (i.e., $p' = p$). The regularized version (31) of $\mathscr{A}_0^0$ will be used in the subsequent numeric calculations.

[2]It is seen best in a momentum representation that there is a contribution to the Volkov state from the free electron without any interaction with the laser field; see the Appendix.

B. Slowly-varying-envelope approximation

The calculations are simplified by utilizing the slowly-varying-envelope approximation (SVEA) of the phase of the $\mathscr{A}_N^M$ functions. This approximation scheme is suitable for long pulses with $\sigma \gg 1$. Typically σ is proportional to the number of laser oscillations under the envelope. For f_1, which is proportional to g [see Eq. (25)], an integration by parts is performed, yielding

$$\int d\phi\, g(\phi)\sin\phi = -g(\phi)\cos\phi + \int d\phi\frac{dg}{d\phi}\cos\phi, \tag{32}$$

$$\int d\phi\, g(\phi)\cos\phi = g(\phi)\sin\phi - \int d\phi\frac{dg}{d\phi}\sin\phi. \tag{33}$$

The SVEA basically means neglecting the second terms containing the derivative of the pulse shape $dg/d\phi$ because it is $O(1/\sigma)$ smaller than the first term. For f_2 [$\propto g^2$; cf. Eq. (26)] we use

$$\int d\phi\, g^2(\phi)\cos^2\phi \approx \frac{1}{2}\int d\phi\, g^2(\phi) + \frac{1}{2}g^2(\phi)\sin\phi\cos\phi, \tag{34}$$

$$\int d\phi\, g^2(\phi)\sin^2\phi \approx \frac{1}{2}\int d\phi\, g^2(\phi) - \frac{1}{2}g^2(\phi)\sin\phi\cos\phi, \tag{35}$$

which becomes particularly handy if $\int d\phi\, g^2$ is known analytically, such as for the hyperbolic secant pulse (8), where $\int d\phi\cosh^{-2}\phi/\sigma = \sigma\tanh(\phi/\sigma) + \text{const}$, or the Gaussian pulse (9), $\int d\phi\exp(-\phi^2/2\sigma^2)^2 = \sqrt{\pi}\sigma\,\mathrm{erf}(\phi/\sigma)/2 + \text{const}$, where $\mathrm{erf}(x)$ is the normalized error function. Finally, the SVEA result for the phase reads

$$f_1 = -\frac{ma_0}{k\cdot p}g(x_+)[p\cdot\epsilon_1\cos\xi\sin\omega x_+ - p\cdot\epsilon_2\sin\xi\cos\omega x_+], \tag{36}$$

$$f_2 = -\frac{m^2a_0^2}{4k\cdot p}\Big[\int^{\omega x_+} d\phi\, g^2(\phi) + g^2(x_+)\cos\omega x_+\sin\omega x_+(\cos^2\xi - \sin^2\xi)\Big], \tag{37}$$

generalizing the approximation scheme of [40] to linear laser polarization.

Even for short pulses, such as for $\sigma = 5$, meaning that there are about five laser oscillations in the pulse, i.e., the pulse length is $\approx$15 fs for $\lambda = 800$ nm, the SVEA is quite a good approximation; see Fig. 2 for selected examples.

C. The spectral distribution of scattered photons and the cross section

In the standard formalism, scattering experiments are thought of as constant streams of particles interacting. Consequently, the square of the S matrix contains a factor T

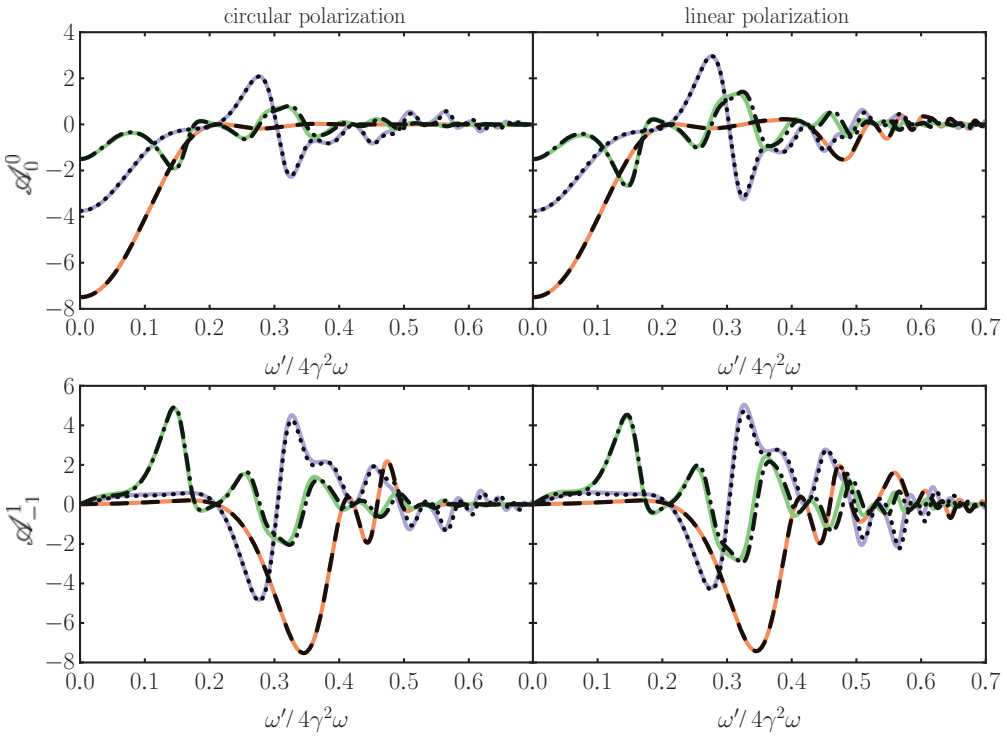

FIG. 2. (Color online) Comparison of the SVEA (dark-colored dashed and dotted curves) and the full numerical results (light-colored solid curves) for different scattering angles $\theta = 0$ (red dashed), $\theta = 1/\gamma$ (blue dotted), and $\theta = 2/\gamma$ (green dash-dotted) for the real parts of the functions $\mathscr{A}_0^0$ (top row) and $\mathscr{A}_{-1}^1$ (bottom row) for $\sigma = 5$ as a function of the normalized frequency $\omega'/4\gamma^2\omega$. Parameters are $a_0 = 1.5$, $\omega = 1.5$ eV, $\gamma = 10^5$. Left (right) panels are for circular (linear) polarization.

which originates from the square of the energy-momentum conservation; it is interpreted as $\delta(P_i - P_f)^2 \to \frac{VT}{(2\pi)^4}\delta(P_i - P_f)$, with the volume V and interaction time T which are both set to infinity. For the purpose of rendering this quantity finite, usually the differential rate per unit time and unit volume, $dw_{i\to f} = \frac{|S_{fi}|^2}{VT}d\Pi$, is considered, where $d\Pi$ denotes the final-state phase space. Here, however, the interaction is happening only within a finite time interval. Because of lacking one δ distribution, the square of the S matrix now reads

$$|S_{fi}|^2 = (2\pi)^3 V\delta(\mathbf{p}'_\perp + \mathbf{k}'_\perp - \mathbf{p}_\perp)\delta(p'_+ + k'_+ - p_+)|N_0\mathscr{M}|^2, \tag{38}$$

where the dependence on the finite interaction time is contained in $\mathscr{M}$. Thus, it is not necessary to define a differential rate per unit time. An appropriate observable is the Lorentz invariant emission probability of photons per unit volume and laser pulse,

$$dN = \frac{|S_{fi}|^2}{V}d\Pi, \tag{39}$$

which has as a classical analog the spectral density of scattered photons in Thomson scattering (cf. [26,37]),

$$\frac{d^2N_{\text{classical}}}{d\omega' d\Omega} = -\frac{\omega'}{16\pi^3}j^*(k')\cdot j(k'), \tag{40}$$

$$j^\mu(k') = e\int d\tau u^\mu(\tau)\, e^{ik'\cdot x(\tau)}, \tag{41}$$

where $u^\mu(\tau)$ and $x^\mu(\tau)$ are the classical four-velocity and orbit from a solution of the Lorentz force equation for a spinless pointlike charge, and $j^\mu(k')$ is the retarded Fourier transform of the electron current. The notion of Thomson scattering is specified to mean this particular calculation scheme. A quantum spectral density is given by the expression

$$\frac{d^2N_{ss'\lambda'}}{d\omega' d\Omega} = \frac{\omega' e^2}{16\pi^3}\frac{|\mathscr{M}_{ss'\lambda'}|^2}{4p_+p'_+} \tag{42}$$

which is (39) integrated over the final electron momentum p' and we note the spin and polarization dependence explicitly here. Averaging over the spin of the incoming electron and summing over the spin of the outgoing electron and the polarization of the outgoing photon yields a quantity which is directly comparable to the classical spectral density,

$$\frac{d^2N_{\text{quantum}}}{d\omega' d\Omega} = \frac{1}{2}\sum_{s,s'=1}^{2}\sum_{\lambda'}\frac{d^2N_{ss'\lambda'}}{d\omega' d\Omega}, \tag{43}$$

where the integrated photon number N_{quantum} is a Lorentz invariant. We can construct a cross section, unambiguously in respect of the pulse shape and pulse length (a different definition of the cross section without this property has been proposed in [41]), by dividing Eq. (43) by the normalized number of photons, N_L, in the laser pulse, i.e.,

$$\frac{d^2\sigma}{d\omega' d\Omega} = \frac{1}{N_L}\frac{d^2N_{\text{quantum}}}{d\omega' d\Omega} \tag{44}$$

with $N_L = \int_{-\infty}^{\infty} dt \frac{\langle|\mathbf{S}|\rangle}{\omega}$, where $\mathbf{S} = \mathbf{E}\times\mathbf{B}$ is the Poynting vector of the laser field, derived from the vector potential (7′),

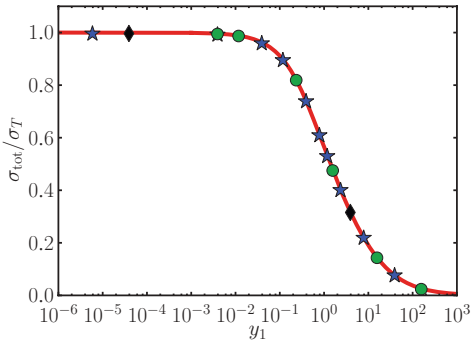

FIG. 3. (Color online) Total cross section $\sigma_{\rm tot}$ for Compton scattering normalized to the Thomson cross section σ_T. Red curve, Klein-Nishina cross section. Symbols, numerically calculated cross section in a pulsed laser field with $a_0 = 0.001$. Blue stars, $\sigma = 20$ for a hyperbolic secant pulse; green circles, $\sigma = 30$ for a Gaussian pulse; black diamonds, $\sigma = 100$ for a Gaussian pulse.

yielding

$$N_L = \frac{\omega}{2}\frac{a_0^2 m^2}{e^2}\int_{-\infty}^{\infty} dt\, g(t)^2 \tag{45}$$

with $\int_{-\infty}^{\infty} dt \cosh^{-2}\phi/\sigma = 2\sigma/\omega$ and $\int_{-\infty}^{\infty} dt \exp(-\phi^2/2\sigma^2)^2 = \sqrt{\pi}\sigma/\omega$ for the pulse shapes (8) and (9), respectively. Using this definition, the total cross section is independent of the pulse shape function g and the pulse length σ in the limit $a_0 \to 0$. This has been checked numerically by a comparison of $\frac{d\sigma}{d\Omega} = \int d\omega' \frac{d^2\sigma}{d\omega' d\Omega}$ with the differential Klein-Nishina cross section [48], or $\sigma_{\rm tot} = \int \frac{d\sigma}{d\Omega} d\Omega$ with the total Klein-Nishina cross section. In particular, in the limit $y_1 \to 0$ we obtain the total Thomson cross section $\sigma_T = 665.25$ mb accurately, as exhibited in Fig. 3 for three different pulse shapes and pulse lengths. In the nonlinear regime, $d^2\sigma/d\omega' d\Omega$ becomes an effective cross section [50] as it explicitly depends on the laser strength parameter a_0 as well as on details of the pulse shape. For a given pulse shape function g, the cross section $\frac{d\sigma}{d\Omega}$ for the first harmonic is a characteristic function, i.e., independent of the pulse length σ. This was confirmed numerically with great accuracy by considering Gaussian pulses with $\sigma = 10, \ldots, 600$.

IV. DISCUSSION

A. Monochromatic limit

In the famous case of monochromatic Compton scattering, the frequency of the scattered photon is uniquely defined by the scattering angle. For a finite temporal laser pulse, however, this tight relation is lost. As outlined in Sec. III C, there is a distribution of the emitted photons for a fixed angle. As an example, we exhibit in the left top panel of Fig. 4 the spectral density $d^2 N_{\rm quantum}/d\omega' d\Omega$ as a function of $\varpi' = \omega'/\omega'_{1,\rm classical}$ for fixed Ω. The vertical thin lines depict the positions of the harmonics for a monochromatic plane wave with infinite duration at the same value of a_0, given by [48]

$$\omega'_\ell = \omega'_{\ell,\rm quantum} = \frac{\ell k\cdot q}{(q+\ell k)\cdot n'}, \tag{46}$$

introducing the intensity-dependent quasimomentum of the electron $q_-^{(\prime)} = p_-^{(\prime)} + b_{p^{(\prime)}} k_-$ with $b_{p^{(\prime)}} = m^2 a_0^2/4k\cdot p^{(\prime)}$ and the dressed mass-shell relation $q^2 = q'^2 = m_*^2 = m^2(1 + a_0^2/2)$, where $p'_- = [(\mathbf{p}'_\perp)^2 + m^2]/2p'_+$ is determined by the free-particle dispersion relation and p'_+ and $\mathbf{p}'_\perp$ are fixed by energy-momentum conservation [see below (26)]. Note that only $p_-^{(\prime)}$, the conjugate momentum to x_+, is modified by an intensity-dependent contribution, i.e., $q_+^{(\prime)} = p_+^{(\prime)}$ and $\mathbf{q}_\perp^{(\prime)} = \mathbf{p}_\perp^{(\prime)}$. The integer ℓ labels the individual harmonics, which are not equidistant in general.

In a pulsed laser field, each harmonic consists of a bunch of spectral "lines" (or subpeaks) visible in the top panels of Fig. 4 with a certain width $\Delta\omega'_\ell$ determined by the maximum value of intensity in the laser pulse. The high-energy tail of each harmonic bunch is given by $\omega'_\ell(a_0 \to 0)$ which is produced at the edges of the laser pulse. The low-energy edge is given by $\omega'_\ell(a_0)$ and accounts for the maximum redshift at the center of the pulse. Thus, the spectral width of each harmonic ℓ is given by

$$\begin{aligned}\Delta\omega'_\ell &= \omega'_\ell(a_0 \to 0) - \omega'_\ell(a_0)\\ &= \omega'_\ell(a_0)\omega'_\ell(a_0 \to 0)\frac{b_p k\cdot n'}{\ell k\cdot p}.\end{aligned} \tag{47}$$

The number of subpeaks in a bunch is proportional to the pulse length σ and the intensity a_0^2. The highest subpeak takes its maximum value at a higher frequency ω' than predicted by (46), and thus at a smaller intensity-dependent redshift than the monochromatic harmonics due to a lower average a_0. Hence, one could say that this maximum is blueshifted as compared to the monochromatic plane wave.

Increasing σ from 20 to 50 does not lead to an accumulation of spectral weight at the nonlinear Compton frequencies as could be expected naively. The number of subpeaks increases but the average shape of the harmonic bunch is more or less the same for $\sigma = 20$ and 50 with the same spectral width. In fact, to obtain the monochromatic limit, it is not efficient to take simply the limit $\sigma \to \infty$. A method with better convergence is to introduce a flat-top area in the pulse. This, however, introduces a second pulse length parameter: The total pulse length now consists of the rise "time" σ and the flat-top "time" τ. The flat-top part of the pulse is parametrized as $g_{\rm box}(\phi;\tau) = \Theta(\phi + \pi\tau)\Theta(\pi\tau - \phi)$, where a factor π is introduced so that τ is comparable to the Gaussian and hyperbolic secant widths σ in terms of laser oscillations under the envelope, and $\Theta(\phi)$ is the Heaviside step function. Then, the complete pulse is parametrized as

$$\begin{aligned}g_{\rm flat\ top}(\phi;\sigma,\tau) = g_{\rm box}(\phi;\tau) &+ g(\phi - \pi\tau)\Theta(\phi - \pi\tau)\\ &+ g(\phi + \pi\tau)\Theta(-\phi - \pi\tau).\end{aligned} \tag{48}$$

The spectrum converges rather fast to sharp peaks centered at the nonlinear Compton frequencies upon increasing τ from 0 to 30 while keeping $\sigma = 20$ constant, as seen in the bottom panel of Fig. 4: The strengths are located at the sharp nonlinear Compton energies. The remaining wiggles around the nonlinear Compton energies vanish upon increasing τ further.

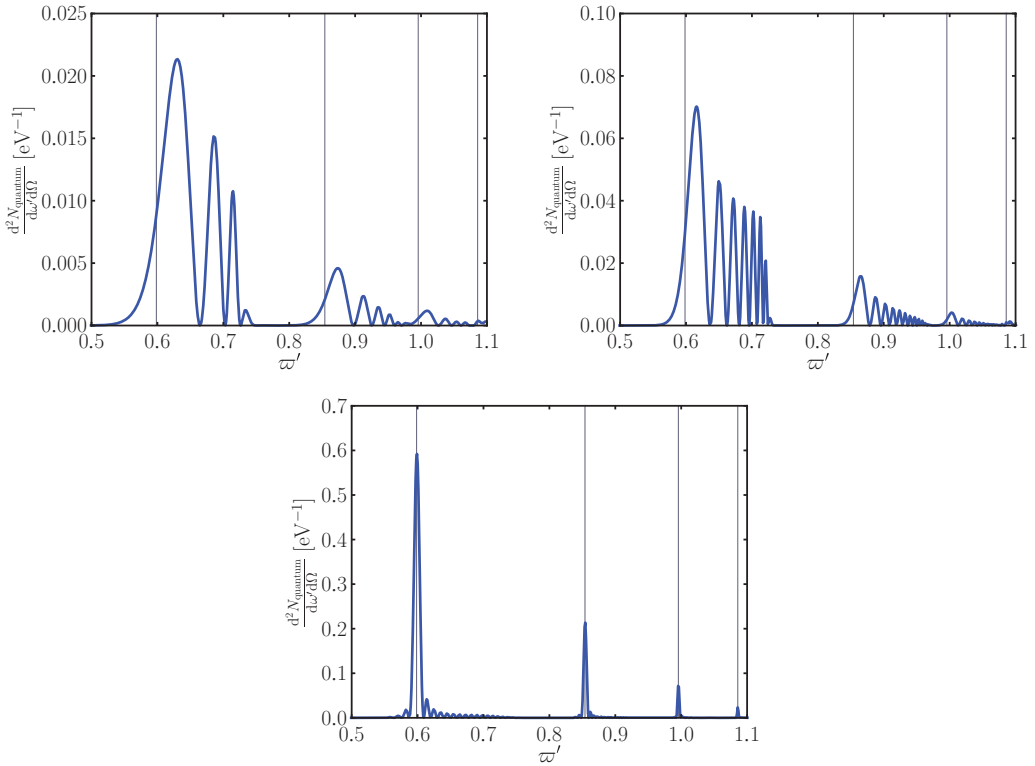

FIG. 4. (Color online) Top panels: Spectral density $d^2N_{\rm quantum}/d\omega' d\Omega$ as a function of the scaled frequency $\varpi' = \omega'/\omega'_{1,\rm classical}$ for a hyperbolic secant pulse with $\sigma = 20$ (left) and 50 (right). Bottom panel: Spectral density for a flat-top pulse with hyperbolic secant edges, $\tau = 30$ and $\sigma = 20$. In all panels $a_0 = 1.0$, $\gamma = 10^5$, $\omega = 1.5$ eV, $\theta = 1/\gamma$, and $\varphi = 0$. The thin vertical lines depict the nonlinear Compton energies defined in Eq. (46).

In the monochromatic limit $\tau \to \infty$, the rising and trailing edges of the pulse shape function become unimportant, i.e., $g \to 1$, and the function H_+ in (27) reduces to

$$H_+ = \frac{1}{2}(k'_- + q'_- - q_-)x_+ + \alpha_1 \sin\omega x_+ - \alpha_2 \cos\omega x_+ - \frac{b_p - b_{p'}}{2}(\cos^2\xi - \sin^2\xi)\sin 2\omega x_+ \tag{49}$$

with $\alpha_i = ma_0(\epsilon_i \cdot p/k \cdot p - \epsilon_i \cdot p'/k \cdot p')$ and identifying the electron quasimomenta $q_-^{(\prime)}$. Upon plugging (49) into (18) and expanding into a Fourier series, one obtains a fourth energy-momentum conservation by integrating over x_+, yielding $q_- + \ell k_- = q'_- + k'_-$. The four energy-momentum constraints together lead again to Eq. (46).

The individual harmonics, consisting of a multitude of subpeaks, begin to overlap if the lower edge of the $(\ell + 1)$st harmonic coincides with the upper edge of the ℓth harmonic, i.e.,

$$\omega'_\ell(a_0 \to 0) \geqslant \omega'_{\ell+1}(a_0). \tag{50}$$

This happens always for sufficiently large values of a_0 and ℓ. The notion of individual harmonics becomes inappropriate, as one rather observes a continuous spectral distribution.

B. Comparison with Thomson scattering

There are different bookkeeping parameters for the characterization of the Thomson regime as the limiting case of the presently considered scenario. One parameter is y_ℓ introduced in Eq. (2). An alternative would be to employ the outgoing momenta instead of the incoming ones, defining $\hat{y} = (\hat{s} - m^2)/m^2$ with $\hat{s} = (p' + k')^2$. When four-momentum conservation holds, both definitions coincide (since k' and p' both depend on ℓ) and $\hat{s}$ coincides with the usual Mandelstam variable s. However, this is not the case here. These recoil parameters are compared in Fig. 5. The parameter $\hat{y}$ is a

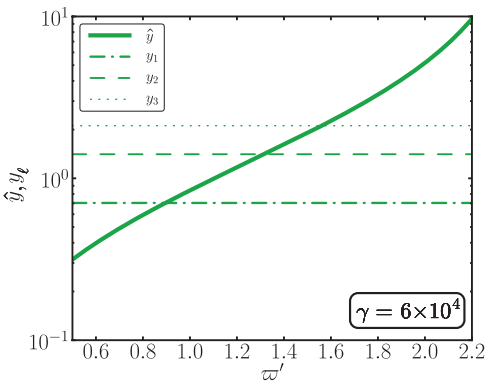

FIG. 5. (Color online) Different recoil parameters $\hat{y}(\omega')$ and y_ℓ for $\ell = 1,2,3$ as functions of the scaled frequency $\varpi' = \omega'/\omega'_{1,\rm classical}$.

function of ω', as it depends on ω' through k',

$$\hat{y} = 2\frac{p'\cdot k'}{m^2} = \frac{2}{m^2}\frac{(p\cdot k')(p\cdot k)}{(p\cdot k - k'\cdot k)} = \frac{2\gamma^2\omega'(1-\mathbf{n}'\cdot\boldsymbol{\beta})}{m\gamma - \omega'\frac{1-\mathbf{n}\cdot\mathbf{n}'}{1-\mathbf{n}\cdot\boldsymbol{\beta}}}, \tag{51}$$

which diverges at $\omega'_\infty = \frac{m\gamma(1-\mathbf{n}\cdot\boldsymbol{\beta})}{1-\mathbf{n}\cdot\mathbf{n}'}$, defining the boundary of phase space. Thus the physical phase space is given by $0 \leqslant \theta < \pi$, $0 \leqslant \varphi < 2\pi$, and $0 < \omega' < \omega'_\infty$. An interpretation of the phase-space boundary will be given in Sec. IV C.

To relate the Compton amplitude with the classical Thomson counterpart it is instructive to consider the phase exponential, e.g., $H_+ \pm \omega x_+$ in $\mathscr{A}^1_{\pm 1}$; cf. Eq. (28). For the sake of simplicity, a backscattering head-on geometry with a circularly polarized laser is assumed in this section. Then, after using some light-cone algebra, the phase reads

$$\begin{aligned} H_+ \pm \omega x_+ &= \left[\frac{k'_- + p'_- - p_-}{2} \pm \omega\right] x_+ \\ &\quad - \left(\frac{m^2a_0^2}{4k\cdot p} - \frac{m^2a_0^2}{4k\cdot p'}\right)\int^{\omega x_+} d\phi\, g^2(\phi) \qquad (52) \\ &= \left[\frac{k'\cdot p}{n_+\cdot p'} \pm \omega\right] x_+ + \frac{k'\cdot k}{(k\cdot p)(k\cdot p')} \\ &\quad \times \frac{m^2a_0^2}{4}\int^{\omega x_+} d\phi\, g^2(\phi). \qquad (53) \end{aligned}$$

Momentum conservation implies $n_+\cdot p' = n_+\cdot p - n_+\cdot k'$. For $n_+\cdot k' \ll n_+\cdot p$, the leading term

$$\begin{aligned} &\left[\frac{k'\cdot p}{n_+\cdot p}x_+ \pm \omega\right] + \frac{k'\cdot k}{(k\cdot p)^2}\frac{m^2a_0^2}{4}\int^{\omega x_+} d\phi\, g^2(\phi) \\ &\quad = k'\cdot x(\tau) \pm \omega x_+ \end{aligned} \tag{54}$$

agrees with the corresponding expression obtained in a classical calculation for Thomson scattering (cf. [37]). The frequency of backscattered photons in monochromatic plane waves is obtained from (46) by neglecting ℓk with respect to q in the denominator, i.e.,

$$\omega'_{\ell,\text{classical}} = \ell\frac{k\cdot q}{q\cdot n'}. \tag{55}$$

In Thomson scattering, the harmonics are always equidistant. A series of plots showing the transition from Thomson to Compton scattering is exhibited in Fig. 6. The deviations between Thomson and Compton scattering are (i) a nonlinear redshift in frequency and (ii) a slight modification in the amplitude starting notably at $y_1 = 0.12$. It is obvious that the redshift is much more pronounced at higher frequencies. Figure 6 quantifies the well-known fact [48] that Compton scattering turns into Thomson scattering in the low-energy limit. For the chosen parameters ($a_0 = 1.0, \omega = 1.5$ eV) the differences become significant for $\gamma \geqslant 10^4$. Very drastic differences are obvious for $\gamma = 10^5$ (bottom right panel of Fig. 6).

C. Scaling properties of the spectral density

The classical and quantum spectral densities for arbitrary pulse shapes can be related by the scaling law

$$\frac{d^2N_\text{classical}}{d\omega' d\Omega}(\omega',\theta) = \frac{1}{\eta}\frac{d^2N_\text{quantum}}{d\omega' d\Omega}(\chi\omega',\theta) \tag{56}$$

with the two scaling factors η and χ which are determined by the monochromatic results. The frequency scaling factor χ is given by

$$\chi = \frac{\omega'_{\ell,\text{quantum}}}{\omega'_{\ell,\text{classical}}} = \frac{n'\cdot u + n'\cdot n\frac{a_0^2}{4n\cdot u}}{n'\cdot u + n'\cdot n\left(\frac{a_0^2}{4n\cdot u} + \ell\frac{\omega}{m}\right)} = \frac{q\cdot n'}{(q+\ell k)\cdot n'} \tag{57}$$

where $u = p/m$. A continuous effective ℓ_eff has to be used, which follows from the inversion of $\omega'_{\ell,\text{quantum}}$, yielding

$$\ell_\text{eff}(\omega') = \frac{\frac{\omega'}{\omega}\left(n'\cdot u + n'\cdot n\frac{a_0^2}{4n\cdot u}\right)}{n\cdot u - n'\cdot n\frac{\omega'}{m}} = \frac{q\cdot k'}{q\cdot k - k'\cdot k}, \tag{58}$$

which simplifies to $\chi = 1 - k'\cdot k/p\cdot k = 1 - k'_+/p_+$. The scaling of the frequency naturally also includes the scaling behavior of the phase-space factor, which is proportional to ω'^2.

The scaling factor η describes the scaling of the differential probabilities defined by

$$\eta = \left(\omega'^{-2}_\text{quantum}\frac{d\sigma_\text{quantum}}{d\Omega}\right)\left(\omega'^{-2}_\text{classical}\frac{d\sigma_\text{classical}}{d\Omega}\right)^{-1}, \tag{59}$$

where the differential cross sections $d\sigma_\text{quantum}$ and $d\sigma_\text{classical}$ are the monochromatic plane-wave cross sections, yielding for circular polarization [37]

$$\eta = \frac{\mathfrak{I}_\ell}{\mathfrak{K}_\ell} = 1 + \frac{x^2}{1+x}\frac{\mathfrak{L}_\ell}{2\mathfrak{L}_\ell - \frac{8}{a_0^2}J_\ell^2(z)}, \tag{60}$$

where $x = (1-\chi)/\chi$, $y_* = 2\ell k\cdot p/m_*^2$, and ℓ_eff has to be used instead of ℓ everywhere. The other definitions are $\mathfrak{L}_\ell = J^2_{\ell+1}(z) + J^2_{\ell-1}(z) - 2J^2_\ell(z)$, $\mathfrak{K}_\ell = -8J^2_\ell(z)/a_0^2 + 2\mathfrak{L}_\ell$, $\mathfrak{I}_\ell = \mathfrak{K}_\ell + \frac{x^2}{1+x}\mathfrak{L}_\ell$, and $z = 2\ell\sqrt{\frac{a_0^2/2}{1+a_0^2/2}}\sqrt{\frac{x}{y_*}(1-\frac{x}{y_*})}$; J_ℓ are Bessel functions of the first kind. In the limit $a_0 \to 0$ one gets

$$\lim_{a_0\to 0}\eta = 1 + \frac{x^2}{1+x}\frac{1}{2 - 4\frac{x}{y_*}\left(1-\frac{x}{y_*}\right)}, \tag{61}$$

which is a good approximation for $a_0 < 1$. For linear laser polarization we expect a similar relation to hold, but with the appropriate linearly polarized monochromatic plane-wave cross section instead.

The scaling function χ is related to the momentum transfer from the incoming electron to the outgoing electron via $p'_+ = \chi p_+$. Thus, χ is the fraction of p_+ momentum transferred from the incoming electron to the outgoing electron p'_+. Furthermore, the fraction of momentum transferred to the photon is $k'_+ = (1-\chi)p_+$ so that $1-\chi$ is another measure of the electron recoil. χ is a monotonically decreasing function of ω'. The point $\chi(\omega') = 0$ corresponds to $p'_+ = 0$ and $k'_+ = p_+$, i.e., the total amount of momentum is transferred from the electron to the photon. Further increase in ω' would render

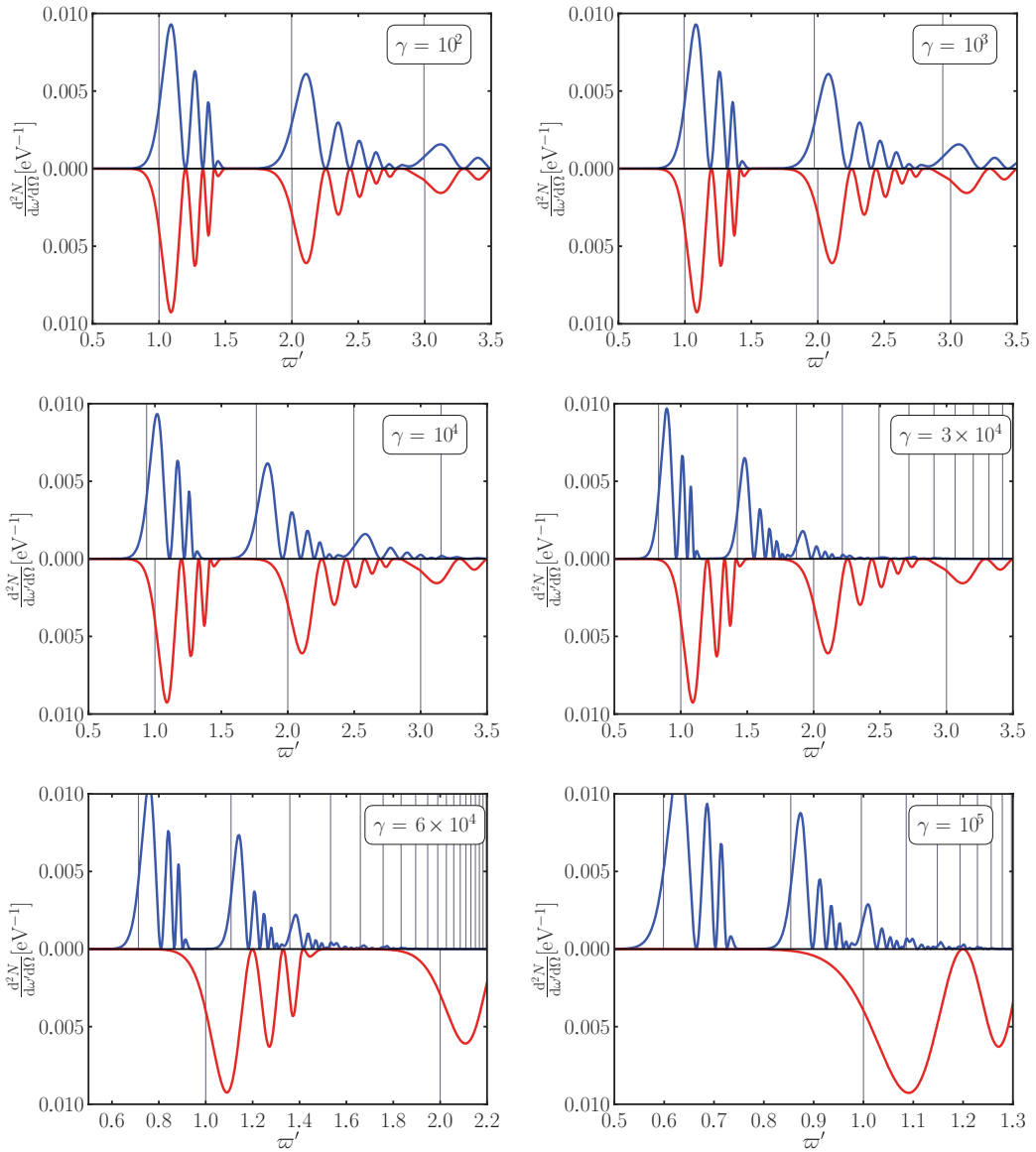

FIG. 6. (Color online) The photon spectrum $d^2N/d\omega' d\Omega$ as a function of the scaled frequency $\varpi' = \omega'/\omega'_{1,\text{classical}}(\theta)$ for $\gamma = 10^2, 10^3, 10^4, 3\times 10^4, 6\times 10^4, 10^5$ (i.e., $y_1 = 0.0012, 0.012, 0.12, 0.35, 0.7, 1.2$) from top left to bottom right for $\theta = 1/2\gamma$ and $\varphi = 0$ for a hyperbolic secant pulse shape. The upper blue curves are for the quantum spectral density $d^2N_{\text{quantum}}/d\omega' d\Omega$ (43) of Compton scattering, whereas the lower red curves are the classical spectral density $d^2N_{\text{classical}}/d\omega' d\Omega$ (40) of Thomson scattering. The vertical gray lines mark the positions of the monochromatic harmonics Eqs. (46) and (55) in the upper and lower halves of each panel, respectively. The other parameters are $a_0 = 1.0$, $\omega = 1.5$ eV, $\sigma = 20$, and $\xi = 0$, i.e., linear laser polarization.

χ as well as p'_+ negative. This defines the boundary of the physical phase space for the outgoing particles. When $p'_+ < 0$, then, due to the free-particle dispersion relation (13), also $p'_- < 0$. This, however, would lead to a negative energy $E_{p'}$ because $E_{p'} = (p'_+ + p'_-)/2 < 0$. Consequently, there exists a maximum frequency ω'_∞, defined by $\chi(\omega'_\infty) = 0$:

$$\omega'_\infty = \frac{p\cdot k}{n'\cdot k} = \frac{m\gamma(1-\mathbf{n}\cdot\boldsymbol{\beta})}{1-\mathbf{n}\cdot\mathbf{n}'}, \tag{62}$$

which can also be obtained as the limit $\lim_{\ell\to\infty}\omega'_\ell = \omega'_\infty$, with ω'_ℓ from Eq. (46). This also coincides with the singularity in $\hat{y}$; see Eq. (51). For the backscattering head-on geometry we obtain $\omega'_\infty = m/2$ for electrons initially at rest and $\omega'_\infty = m\gamma(1+\beta)/2 \approx E_p$ for ultrarelativistic particles, i.e., the maximum backscattered frequency is determined by the energy of the incoming electron. The momentum components p'_+, p'_-, and $E_{p'}$ are depicted in the left panel of Fig. 7 as functions of ω' in the electron rest frame. The right panel of Fig. 7 shows the dependence of ω'_∞ on the scattering angle θ. It takes its minimum at the backscattering direction $\theta = 0$ and goes to infinity in the limit $\theta \to \pi$, i.e., forward scattering.

D. Further differences between the classical and QED calculations

As demonstrated in the preceding sections and quantified by the scaling law, the main difference between the spectral densities of Thomson and Compton scattering is caused by

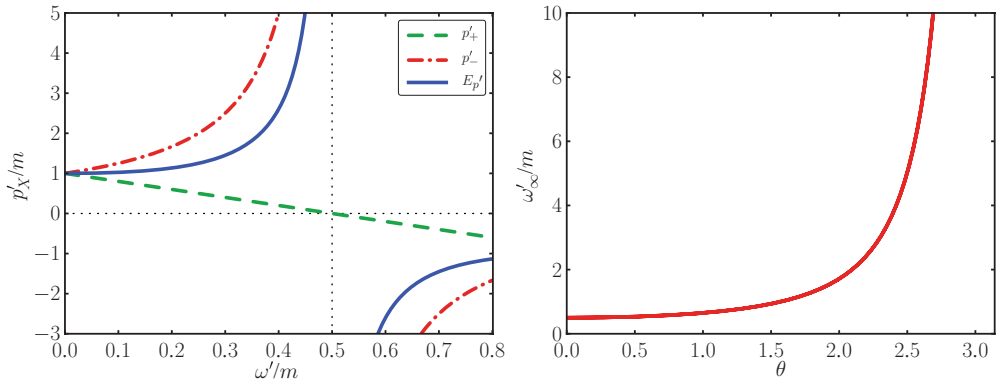

FIG. 7. (Color online) Left panel: Different components of the outgoing electron momentum p'_X as a function of frequency ω' for backscattering geometry in the rest frame of the incoming electron. Shown are p'_- (red, dash-dotted), p'_+ (green, dashed), and $p'_0 = E_{p'}$ (blue, solid). The physical phase space has its support at $\chi > 0$, i.e., for $0 < \omega'/m < 0.5 = \omega'_\infty/m$ in this case. Right panel: Maximum frequency ω'_∞ as function of scattering angle θ, where $\theta = 0$ denotes the backscattering direction.

the proper treatment of the electron recoil in the latter. Additionally, there is another regime where the quantum description goes beyond a classical calculation, even if $\hat{y} \ll 1$, where the total Thomson and Compton cross sections are equal in leading order. This happens in regions of phase space where individual harmonics are overlapping [see Eq. (50)]. There, the subpeaks in the quantum calculation show completely different patterns in comparison to a classical calculation; see Fig. 8. Consequently, the scaling law may not be applied where harmonics are overlapping. For a better orientation, the spectral ranges of the individual harmonics are marked in Fig. 8, where the lower (upper) edges are depicted by dotted (dashed) lines. Due to the finite pulse length σ, the actual spectral distribution reaches over these edges by $O(\tilde{\sigma})$, where $\tilde{\sigma} = \gamma^2(1+\beta)^2/\sigma$. The gray shaded areas mark the overlapping regions with a width of $2\tilde{\sigma}$.

The generation of the subpeaks can be described as an interference effect [37]. Thus, when the harmonics overlap, for a fixed value of ω' there are contributions from different harmonics and their interference reacts very sensitively to subtle changes in the phase of the $\mathscr{A}_N^M$ functions; see Eqs. (53) and (54). The difference in the spectral distributions looks qualitatively similar to Fig. 1 of [38], where the influence of the classical radiation reaction force on the spectrum was studied. The radiation reaction force also provides an electron recoil in the classical calculation, slightly changing the phases and leading to a modified spectrum.

V. SUMMARY

In this paper, we discussed nonlinear Compton scattering in the Furry picture and employed light-cone coordinates for temporally shaped laser pulses. We emphasized the structure of the Volkov wave functions in a pulsed laser field. The S matrix element for nonlinear Compton scattering was evaluated in the framework of Volkov states within the Furry picture. An expression for the cross section which is unambiguously defined in respect of the pulse shape and pulse length was presented.

We focused on the differences between classical calculations of nonlinear Thomson scattering and quantum calculations of nonlinear Compton scattering. In both cases, spectral broadening and harmonic substructures have been found, which are, however, shifted in the quantum calculation. These harmonic substructures, still lacking an experimental verification, are interpreted as an interference effect. We found that for small recoil parameter y_ℓ defined in (2), i.e., $y_\ell \ll 1$,

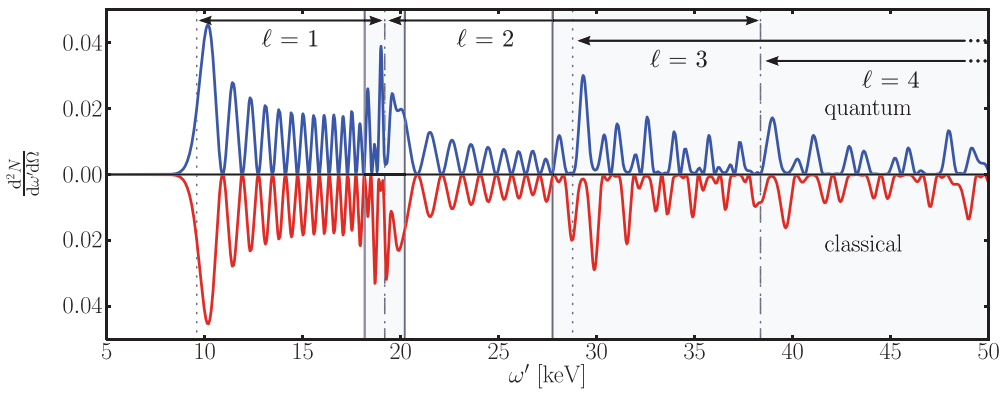

FIG. 8. (Color online) Comparison of the quantum (upper, $d^2N_{\text{quantum}}/d\omega' d\Omega$) and classical (lower, $d^2N_{\text{classical}}/d\omega' d\Omega$) spectral distributions as a function of ω' for fixed angles $\theta = 1/\gamma, \varphi = 0$. The overlap regions of different "harmonics" are highlighted as gray shaded areas. Parameters are $\sigma = 50$, $\omega = 1.5$ eV, $a_0 = 2.0$, $\gamma = 80$, i.e., $\hat{y} \leqslant 2.5 \times 10^{-3}$.

the differential quantum transition probability in many cases coincides with the classical Thomson scattering result also for pulsed laser fields, i.e., quantum effects are mostly negligible in this regime. Also, the total Compton cross section coincides with the Thomson cross section σ_T for $y_\ell < 10^{-2}$.

As a main result, we presented a scaling law, connecting the classical and quantum spectral densities for arbitrary y_ℓ, e.g., $y_\ell > 10^{-2}$, relating the classical and quantum results. The remarkable feature is that the substructures of individual harmonics are also simply scaled. One might speculate that the scaling law may also be applied for arbitrary laser beams, in particular, for strongly focused beams. Hence, it might serve as a tool for adding recoil effects to results obtained within classical Thomson scattering models.

Furthermore, we also found regions in phase space where the differential probabilities for Thomson and Compton scattering are different, although $y_\ell < 10^{-2}$ and the total cross sections coincide. This happens for sufficiently large values of a_0, when the individual harmonics are overlapping. In these regions of phase space, both spectral densities show a different, almost erratic behavior. This observation is in qualitative agreement with previous studies of the effect of the radiation reaction force on the spectrum of nonlinear Thomson scattering. The radiation reaction force introduces an electron recoil in Thomson scattering to the classical picture. Of course, the scaling law is not applicable in the regions where the spectral densities show this erratic behavior.

ACKNOWLEDGMENTS

The authors gratefully acknowledge stimulating discussions with T. E. Cowan and K. Chouffani.

APPENDIX: VOLKOV STATES IN MOMENTUM SPACE

Here, we provide the Fourier transformation of the Volkov state (5) to obtain the matrix element for nonlinear Compton scattering as a convolution in momentum space. For the Fourier transformation we use the convention

$$\tilde{F}(Q) = \int d^4x F(x) e^{ix\cdot Q}, \quad F(x) = \int \frac{d^4Q}{(2\pi)^4} \tilde{F}(Q) e^{-ix\cdot Q}, \tag{A1}$$

where the scalar product has to be taken with respect to the metric (12). The Fourier transform of the Volkov matrix $C_p(x)$ [see Eq. (15)] reads

$$\begin{aligned}\tilde{C}_p(\mathbf{Q}_\perp, Q_+, Q_-) &= (2\pi)^3 \delta^2(\mathbf{Q}_\perp - \mathbf{p}_\perp)\delta(Q_+ - p_+) \\ &\quad \times \{\mathcal{G}_0(Q_-) + d_p \not{k}[\not{\epsilon}_- \mathcal{G}_1(Q_-) + \not{\epsilon}_+ \mathcal{G}_{-1}(Q_-)]\}\end{aligned} \tag{A2}$$

with

$$\mathcal{G}_N(Q_-) = \int dx_+ e^{\frac{i}{2}(Q_- - p_-)x_+} g^{|N|}(x_+) e^{iN\omega x_+ + if(x_+)}. \tag{A3}$$

The functions $\mathcal{G}_N$ describe the nontrivial, pulse-dependent momentum distribution of the Volkov wave function. In particular, $\mathcal{G}_0$ has to be regularized similarly to (31) to allow for a numerical evaluation, where a contribution $\propto \delta(Q_- - p_-)$ emerges, which describes the free part of the Volkov electron without any interaction with the laser pulse. In total, this part of the wave function behaves as $\propto \delta^4(Q - p)$ which is just a free monochromatic electron wave (momentum eigenfunction) in momentum representation.

Using the Fourier representation of the Volkov state, the matrix element for nonlinear Compton scattering (16) reads

$$\begin{aligned}S_{fi} = N_0 (2\pi)^3 \delta^2(\mathbf{p}'_\perp + \mathbf{k}'_\perp - \mathbf{p}_\perp)\delta(p'_+ + k'_+ - p_+) \times \\ \times \left[\mathcal{T}_0^0(\mathcal{G}_0^* \star \mathcal{G}_0) + \mathcal{T}_1^1(\mathcal{G}_0^* \star \mathcal{G}_1)\right. \\ + \mathcal{T}_{-1}^1(\mathcal{G}_0^* \star \mathcal{G}_{-1}) + \mathcal{T}_0^2(\mathcal{G}_1^* \star \mathcal{G}_1) \\ \left. + \mathcal{T}_2^2(\mathcal{G}_{-1}^* \star \mathcal{G}_1) + \mathcal{T}_{-2}^2(\mathcal{G}_1^* \star \mathcal{G}_{-1})\right]\end{aligned} \tag{A4}$$

with the convolution

$$(\mathcal{G}_N^* \star \mathcal{G}_M) \equiv \int \frac{dQ_-}{4\pi} \mathcal{G}_N^*(Q_- - k'_-)\mathcal{G}_M(Q_-). \tag{A5}$$

Comparing (A4) with (29) and (30), we find

$$\begin{aligned}\mathcal{A}_0^0 &= \mathcal{G}_0^* \star \mathcal{G}_0, \quad \mathcal{A}_{\pm1}^1 = \mathcal{G}_0^* \star \mathcal{G}_{\pm1}, \\ \mathcal{A}_0^2 &= \mathcal{G}_1^* \star \mathcal{G}_1, \quad \mathcal{A}_{\pm2}^2 = \mathcal{G}_{\mp1}^* \star \mathcal{G}_{\pm1}.\end{aligned} \tag{A6}$$

The representation (A4) of the Compton amplitude together with (A5) furnishes another interpretation of the subpeaks in the Compton rate as the overlap of the momentum distributions of incoming and outgoing Volkov states.

[1] A. Strickland and G. Mourou, Opt. Commun. **56**, 219 (1985).
[2] ELI project homepage, [http://www.extreme-light-infrastructure.eu].
[3] H. R. Reiss, J. Math. Phys. **3**, 59 (1962).
[4] A. I. Nikishov and V. I. Ritus, Zh. Eksp. Teor. Fiz. **46**, 776 (1963) [Sov. Phys. JETP **19**, 529 (1964)].
[5] A. I. Nikishov and V. I. Ritus, Zh. Eksp. Teor. Fiz. **46**, 1768 (1964) [Sov. Phys. JETP **19**, 1191 (1964)].
[6] A. I. Nikishov and V. I. Ritus, Zh. Eksp. Teor. Fiz. **47**, 1130 (1964) [Sov. Phys. JETP **20**, 757 (1965)].
[7] I. I. Goldman, Phys. Lett. **8**, 103 (1964).
[8] N. B. Narozhnyi, A. I. Nikishov, and V. I. Ritus, Zh. Eksp. Teor. Fiz. **47**, 930 (1964) [Sov. Phys. JETP **20**, 622 (1965)].
[9] L. S. Brown and T. W. B. Kibble, Phys. Rev. **133**, A705 (1964).
[10] T. W. B. Kibble, Phys. Rev. **138**, B740 (1965).
[11] K. T. McDonald, DOE Report No. DOE/ER/3072-38 (unpublished), [www.hep.princeton.edu/~mcdonald/e144/prop.pdf].
[12] R. C. Fernow *et al.*, DOE Report No. DOE/ER/3072-55 (unpublished).
[13] Y. Y. Lau, F. He, D. Umstadter, and R. Kowalczyk, Phys. Plasmas **10**, 2155 (2003).
[14] G. A. Mourou, T. Tajima, and S. V. Bulanov, Rev. Mod. Phys. **78**, 309 (2006).
[15] Y. I. Salamin, S. X. Hu, K. Z. Hatsagortsyan, and C. H. Keitel, Phys. Rep. **427**, 41 (2006).

[16] M. Marklund and P. K. Shukla, Rev. Mod. Phys. **78**, 591 (2006).
[17] V. I. Ritus and P. N. Lebedeva, Akad. Nauk SSSR **111**, 5 (1979).
[18] T. Heinzl and A. Ilderton, Opt. Commun. **282**, 1879 (2009).
[19] T. J. Englert and E. A. Rinehart, Phys. Rev. A **28**, 1539 (1983).
[20] S.-y. Chen, A. Maksimchuk, and D. Umstadter, Nature (London) **396**, 653 (1998).
[21] M. Babzien *et al.*, Phys. Rev. Lett. **96**, 054802 (2006).
[22] H. Schwoerer, B. Liesfeld, H.-P. Schlenvoigt, K.-U. Amthor, and R. Sauerbrey, Phys. Rev. Lett. **96**, 014802 (2006).
[23] C. Bamber *et al.*, Phys. Rev. D **60**, 092004 (1999).
[24] C. Bula *et al.* (E144 Collaboration), Phys. Rev. Lett. **76**, 3116 (1996).
[25] D. L. Burke *et al.*, Phys. Rev. Lett. **79**, 1626 (1997).
[26] E. S. Sarachik and G. T. Schappert, Phys. Rev. D **1**, 2738 (1970).
[27] E. Esarey, S. K. Ride, and P. Sprangle, Phys. Rev. E **48**, 3003 (1993).
[28] R. L. Schoenlein *et al.*, Science **274**, 236 (1996).
[29] K. Chouffani, D. Wells, F. Harmon, and G. Lancaster, Nucl. Instrum. Methods Phys. Res. A **495**, 95 (2002).
[30] A. Debus *et al.*, Proc. SPIE **7359**, 735908 (2009).
[31] W. P. Leemans, R. W. Schoenlein, P. Volfbeyn, A. H. Chin, T. E. Glover, P. Balling, M. Zolotorev, K. J. Kim, S. Chattopadhyay, and C. V. Shank, Phys. Rev. Lett. **77**, 4182 (1996).
[32] F. Sauter, Z. Phys. **69**, 742 (1931).
[33] FACET project home page [http://facet.slac.stanford.edu/].
[34] G. A. Krafft, Phys. Rev. Lett. **92**, 204802 (2004).
[35] J. Gao, Phys. Rev. Lett. **93**, 243001 (2004).
[36] F. V. Hartemann, A. L. Troha, N. C. Luhmann Jr., and Z. Toffano, Phys. Rev. E **54**, 2956 (1996).
[37] T. Heinzl, D. Seipt, and B. Kämpfer, Phys. Rev. A **81**, 022125 (2010).
[38] F. V. Hartemann and A. K. Kerman, Phys. Rev. Lett. **76**, 624 (1996).
[39] R. A. Neville and F. Rohrlich, Phys. Rev. D **3**, 1692 (1971).
[40] N. B. Narozhnyi and M. S. Fofanov, JETP **83**, 14 (1996).
[41] M. Boca and V. Florescu, Phys. Rev. A **80**, 053403 (2009).
[42] F. Mackenroth, A. Di Piazza, and C. H. Keitel, Phys. Rev. Lett. **105**, 063903 (2010).
[43] J. Peatross, C. Müller, K. Z. Hatsagortsyan, and C. H. Keitel, Phys. Rev. Lett. **100**, 153601 (2008).
[44] M. Ruf, G. R. Mocken, C. Müller, K. Z. Hatsagortsyan, and C. H. Keitel, Phys. Rev. Lett. **102**, 080402 (2009).
[45] C. Harvey, T. Heinzl, and A. Ilderton, Phys. Rev. A **79**, 063407 (2009).
[46] W. H. Furry, Phys. Rev. **81**, 115 (1951).
[47] P. Panek, J. Z. Kamiński, and F. Ehlotzky, Opt. Commun. **213**, 121 (2002).
[48] V. B. Berestetsky, E. M. Lifshitz, and L. P. Pitaevsky, *Relativistische Quantentheorie (Lehrbuch der Theoretischen Physik, Band 4)* (Akademie Verlag, Berlin, 1982).
[49] D. Seipt and B. Kämpfer, e-print arXiv:1010.3301v1.
[50] D. Yu. Ivanov, G. L. Kotkin, and V. G. Serbo, Eur. Phys. J. C **36**, 127 (2004).